

2023 summer warmth unparalleled over the past 2,000 years

<https://doi.org/10.1038/s41586-024-07512-y>

Jan Esper^{1,2✉}, Max Torbenson¹ & Ulf Büntgen^{2,3,4}

Received: 16 January 2024

Accepted: 2 May 2024

Published online: 14 May 2024

 Check for updates

Including an exceptionally warm Northern Hemisphere summer^{1,2}, 2023 has been reported as the hottest year on record^{3–5}. However, contextualizing recent anthropogenic warming against past natural variability is challenging because the sparse meteorological records from the nineteenth century tend to overestimate temperatures⁶. Here we combine observed and reconstructed June–August surface air temperatures to show that 2023 was the warmest Northern Hemisphere extra-tropical summer over the past 2,000 years exceeding the 95% confidence range of natural climate variability by more than 0.5 °C. Comparison of the 2023 June–August warming against the coldest reconstructed summer in CE 536 shows a maximum range of pre-Anthropocene-to-2023 temperatures of 3.93 °C. Although 2023 is consistent with a greenhouse-gases-induced warming trend⁷ that is amplified by an unfolding El Niño event⁸, this extreme emphasizes the urgency to implement international agreements for carbon emission reduction.

Observational data from around the world show that the 2023 summer temperatures were extremely warm across the Northern Hemisphere landmasses and that these conditions continued globally until the end of the year (ref. 9). This conclusion came without surprise as several regional heatwaves, exceeding any daily or weekly instrumental measurements, were reported throughout the boreal summer of 2023 (ref. 10). These conditions were subsequently propagated by a developing El Niño event distributing warm surface waters across the equatorial Pacific¹¹ superimposed on rising greenhouse gas concentrations in the atmosphere of Earth¹².

2023 in the observational record

By using the Berkeley Earth aggregated measurements from thousands of meteorological stations (Methods and Extended Data Figs. 1 and 2), we show that the 2023 June–August (JJA) temperatures over the 30–90° N landmass were 2.07 °C warmer than the early instrumental mean between 1850 and 1900 (Table 1). This finding demonstrates not only that 2023 saw the warmest-ever recorded summer across the Northern Hemisphere extra-tropics but also that the 2015 Paris Agreement¹³ to constrain warming globally to 1.5 °C has already been superseded at this limited spatial scale.

Calculations of these temperature ranges are, however, challenged by inconsistencies in the available meteorological network¹⁴ and higher uncertainties of early instrumental measurements¹⁵. A large-scale comparison of station and proxy data recently showed that the nineteenth-century temperature baseline used to contextualize global warming was several tenths of a degree Celsius colder than the expected value⁶. This bias arises from a lack of station records in remote regions and direct insolation effects on inadequately sheltered thermometers^{16,17}. These offsets fundamentally question the calculation of temperature ranges considered in the

2015 Paris Agreement using observational data back to as early as 1850 (ref. 18).

To mitigate these uncertainties in the early instrumental network, we focused our estimate on the 30–90° N latitudinal band, in which most of the long-term meteorological stations are located¹⁹. However, even at this restricted spatiotemporal scale, the number of station records incorporated in the global datasets^{20–22} falls from thousands during the twenty-first century to only 58 for 1850–1900, of which 45 are in Europe. We, therefore, combined the 30–90° N observational measurements with a community ensemble of annually resolved and absolutely dated reconstructions of Northern Hemisphere extra-tropical summer temperatures²³ and considered the large uncertainties of proxy-based temperature estimates to provide a robust Common Era context for 2023 (refs. 24–28) (Methods and Extended Data Figs. 4–6).

2023 warming in Common Era context

Comparison of the community ensemble reconstruction and observational Northern Hemisphere 30–90° N JJA temperatures shows an offset of 0.24 °C from 1850 to 1900 supporting the conclusion of a systematic warm bias in early instrumental observations^{6,16,17} (Methods and Extended Data Fig. 3). This offset is here considered by showing the observed and reconstructed summer temperatures with respect to the 1850–1900 reconstruction mean (Fig. 1). The combined time series show that the summer of 2023 exceeded the long-term pre-instrumental mean from 1 to 1890 by 2.20 °C. The shift from 2.07 °C based on adjusted observational data, to 2.20 °C when referring to the pre-1850 period arises from the extended cold periods of the Common Era, such as the Late Antique Little Ice Age in the mid-sixth century²⁹ and the climax of the Little Ice Age in the early nineteenth century³⁰. Most of these cold phases, as well as the coldest individual summers (highlighted in

¹Department of Geography, Johannes Gutenberg University, Mainz, Germany. ²Global Change Research Institute of the Czech Academy of Sciences, Brno, Czech Republic. ³Department of Geography, University of Cambridge, Cambridge, UK. ⁴Department of Geography, Masaryk University, Brno, Czech Republic. ✉e-mail: esper@uni-mainz.de

Table 1 | Record temperatures

	Year	JJA temperature	95% range
Observations	2023	2.07 °C	
Warmest	2016	1.93 °C	
	1998	1.49 °C	
Pre-instrumental	246	0.88 °C	-0.03 to 1.50 °C
Warmest	282	0.72 °C	-0.14 to 1.56 °C
	1061	0.72 °C	-0.10 to 1.53 °C
	986	0.70 °C	-0.15 to 1.28 °C
Coldest	1642	-1.24 °C	-0.15 to -1.84 °C
	1601	-1.37 °C	-0.75 to -2.16 °C
	627	-1.47 °C	-0.32 to -3.37 °C
	536	-1.86 °C	-0.31 to -3.08 °C

Warmest observed, and coldest and warmest reconstructed JJA land temperatures all expressed as anomalies from the reconstructed 1850–1900 mean. The instrumental values have been adjusted considering the 1850–1900 offset between (colder) reconstructed and (warmer) observed temperatures (Methods and Extended Data Fig. 3). The 95% uncertainty range is derived from the spread among the 15 reconstruction ensemble members²³. The difference between the warmest pre-instrumental year (CE 246) and 2023 is 1.19 °C and between the coldest pre-instrumental year (CE 536) and 2023 is 3.93 °C.

Fig. 1b), followed large, sulfur-rich volcanic eruptions, the stratospheric aerosol veils of which triggered rapid surface cooling^{31,32}.

We list the pre-instrumental cold and warm extremes in Table 1 as they represent the full spectrum of naturally forced climate variability during the Common Era period. The 95% uncertainty range reflects the differences between the 15 reconstruction ensemble members driven by varying methodological choices of the involved research teams and fading proxy network replication back in time²³. If we relate 2023 to the coldest reconstructed summer in CE 536 (-1.86 °C), which was influenced by a large volcanic eruption²⁹, the maximum range of pre-Anthropocene-to-2023 temperatures is 3.93 °C. The range between the warmest naturally forced summer of CE 246 (0.88 °C), which occurred during the Late Roman Warm Period³³ and in 2023 (2.07 °C) during the Anthropocene is 1.19 °C. Even when considering the relatively large uncertainty of -0.03 °C to 1.50 °C for CE 246, the summer of 2023 exceeded this range of natural climate variability

by a minimum of more than 0.5 °C. This approximation provides an estimate of the greenhouse gas contribution to a single extreme year and could be considered conservative as it is derived from the highest pre-instrumental summer temperature of the past 2,000 years.

Forcing of recent temperature extremes

Large-scale temperature anomalies can be amplified by extreme states of the El Niño Southern Oscillation³⁴. This is shown by comparing the 30–90° N JJA temperatures with Nino3.4 sea surface temperatures³⁵ over the past 60 years, which shows that the most notable warming steps are associated with strong El Niño events (Fig. 2). The extreme 2023 summer heat exceeded the previous El-Niño-affected summer of 2016 by 0.23 °C. However, the monthly Nino3.4 index suggests that the ongoing event has yet to unfold. The current El Niño is forecasted to extend into early summer of 2024 (ref. 36). Furthermore, previous anomalies (highlighted in red in Fig. 2a) show a delay between extreme El Niño Southern Oscillation conditions and large-scale temperature deviations³⁷, suggesting that 2024 will see temperature records broken again.

The step change in El-Niño-affected Northern Hemisphere summer temperatures highlighted in Fig. 2a includes some inconsistencies worthy of discussion. First, the persistent El Niño conditions culminating in 1992 did not stimulate record warmth as the event coincided with the eruption of Mount Pinatubo in June 1991 (ref. 38), which released substantial amounts of sulfur into the stratosphere and scattered sunlight and caused summer cooling in the subsequent years³⁹. Smaller but still significant eruptions occurred in 1963 (Mount Agung) and 1982 (El Chichón)^{40,41}. Second, the temperatures recorded in 1998, and affected by an extreme El Niño event, were subsequently not exceeded in 2003, thereby contributing to what has been described as the temperature hiatus⁴², a decade during which global temperatures did not increase beyond the level of the late twentieth century⁴³. The hiatus ended in 2010 when a slightly stronger El Niño than in 2003 occurred and, along with the underlying trend in greenhouse gas concentrations, resulted in average 30–90° N JJA temperatures exceeding those of summer of 1998 by 0.36 °C. Third, the lack of warming until the mid-1980s was probably affected by global dimming⁴⁴, a phenomenon referring to changes in atmospheric transmission and cloudiness because of increased releases of aerosols during post-war economic

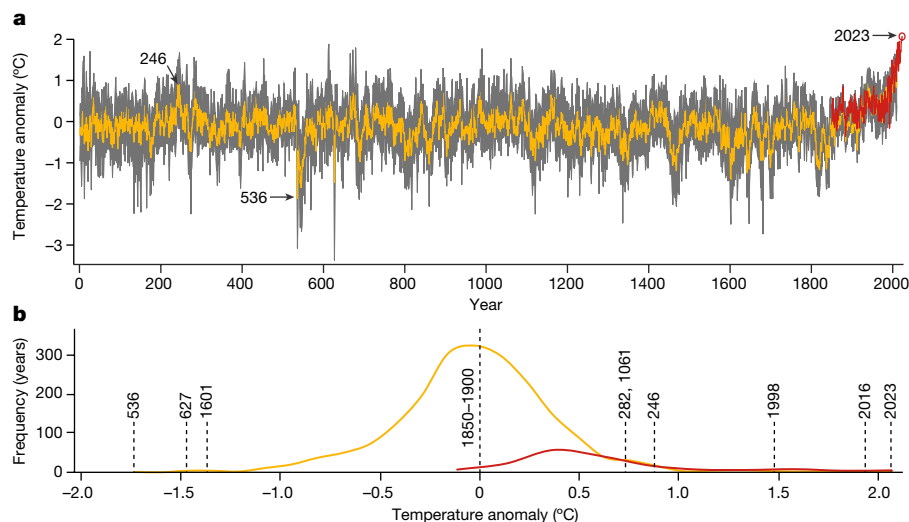


Fig. 1 | 2023 in the context of the past 2,000 years. a, Instrumental JJA land temperatures (red; Berkeley Earth)²⁰ shown together with the ensemble reconstruction mean (yellow) and 95% uncertainty range derived from the variance among ensemble members (grey)²³. Ensemble reconstructions were

scaled from 1901 to 2010 against observations and expressed as anomalies with respect to the 1850–1900 mean (Methods). **b**, Frequency distributions of the observed and reconstructed temperature anomalies (0 °C = 1850–1900 mean) with exceptionally cold and warm summers highlighted.

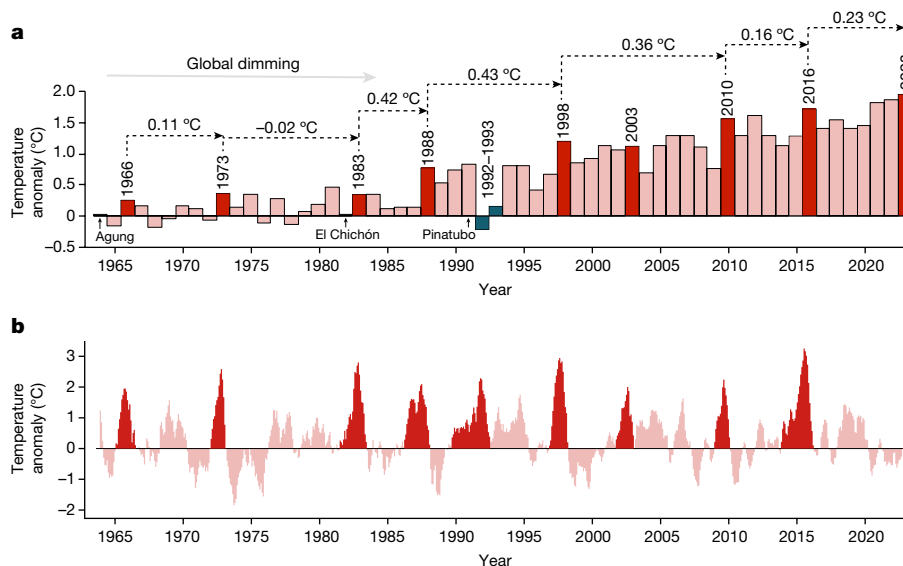


Fig. 2 | Forcing of modern-day temperatures. a, Instrumental Northern Hemisphere summer temperatures (CRUTEM5)²¹ with years affected by strong El Niño conditions highlighted in red and years affected by the Mount Pinatubo eruption in grey. The grey arrow indicates the period of global dimming ending in the mid-1980s (ref. 44), and the dashed arrows indicate temperature steps

between strong El Niño events (except for 2003). **b**, Niño3.4 sea surface temperatures³⁵ with El Niño events of at least 2 °C highlighted in red (data accessed using the KNMI Climate Explorer at <https://climexp.knmi.nl/start.cgi>). Data are shown as anomalies from the means of 1891–1920.

expansion. This negative radiative forcing faded in the 1980s when effective measures for sulfur scrubbing were established in Europe and North America⁴⁵.

Although the variance of Northern Hemisphere land temperatures is systematically larger than that of global land and sea surface temperatures (Extended Data Fig. 2), the sub-hemispheric pre-Anthropocene-to-2023 warming reported here cannot be transferred to global scales. This is because spatially varying warming rates among high compared with low latitudes and land compared with sea surfaces challenge simple linear extrapolations, and multiproxy reconstructions of global temperatures⁴⁶ are constrained by the integration of lower-resolution archives and seasonal signals⁴⁷. However, the pre-Anthropocene-to-2023 estimate of 2.20 °C established here for Northern Hemisphere extra-tropical summers demonstrates the unparalleled nature of present-day warmth at large spatial scales and reinforces calls for immediate action towards net zero emissions.

Online content

Any methods, additional references, Nature Portfolio reporting summaries, source data, extended data, supplementary information, acknowledgements, peer review information; details of author contributions and competing interests; and statements of data and code availability are available at <https://doi.org/10.1038/s41586-024-07512-y>.

1. McKie, R. World experiences hottest week ever recorded and more is forecast to come. *The Guardian* <https://www.theguardian.com/world/2023/jul/16/red-alert-the-worlds-hottest-week-ever-and-more-is-to-forecast-to-come> (16 July 2023).
2. Sands, L. This July 4 was hot. Earth's hottest day on record, in fact. *The Washington Post* (5 July 2023).
3. Poynting, M. & Rivault, E. 2023 confirmed as world's hottest year on record. *BBC* (9 January 2024).
4. Copernicus. 2023 is the hottest year on record, with global temperatures close to the 1.5 °C limit. *Copernicus* (9 January 2024).
5. Bardan, R. NASA analysis confirms 2023 as warmest year on record. *NASA* <https://www.nasa.gov/news-release/nasa-analysis-confirms-2023-as-warmest-year-on-record> (12 January 2024).
6. Schneider, L., Konter, O., Esper, J. & Anchukaitis, K. J. Constraining the nineteenth-century temperature baseline for global warming. *J. Climate* **36**, 6261–6272 (2023).
7. Friedlingstein, P. et al. Global carbon budget 2023. *Earth Syst. Sci. Data* **15**, 5301–5369 (2023).

8. van Oldenborgh, G. J. et al. Defining El Niño indices in a warming climate. *Environ. Res. Lett.* **16**, 044003 (2021).
9. Rohde, R. *Global Temperature Report for 2023* (Berkeley Earth, 2024).
10. Zachariah, M. et al. *Extreme heat in North America, Europe and China in July 2023 Made Much More Likely by Climate Change* <https://www.worldweatherattribution.org/extreme-heat-in-north-america-europe-and-china-in-july-2023-made-much-more-likely-by-climate-change> (World Weather Attribution, 2023).
11. NOAA Climate Prediction Center. *El Niño/La Niña Home* (NOAA Climate Prediction Center, 2024).
12. NOAA Global Monitoring Laboratory. *Trends in Atmospheric Carbon Dioxide* (Global Monitoring Laboratory, 2024).
13. United Nations. *7. d Paris Agreement*, Treaty Series, Vol. 3156, 79 (United Nations, 2015).
14. Jones, P. The reliability of global and hemispheric surface temperature records. *Adv. Atmos. Sci.* **33**, 269–282 (2016).
15. Frank, D., Büntgen, U., Böhm, R., Maugeri, M. & Esper, J. Warmer early instrumental measurements versus colder reconstructed temperatures: shooting at a moving target. *Quat. Sci. Rev.* **26**, 3298–3310 (2007).
16. Parker, D. E. Effects of changing exposure of thermometers at land stations. *Int. J. Climatol.* **14**, 1–31 (1994).
17. Trewin, B. Exposure, instrumentation, and observing practice effects on land temperature measurements. *Wiley Interdiscip. Rev. Clim. Change* **1**, 490–506 (2010).
18. Masson-Delmotte, V. P. et al. (eds) *Climate Change 2021: The Physical Science Basis. Contribution of Working Group I to the Sixth Assessment Report of the Intergovernmental Panel on Climate Change* (Cambridge Univ. Press, 2021).
19. Menne, M. J., Williams, C. N., Gleason, B. E., Rennie, J. J. & Lawrimore, J. H. The Global Historical Climatology Network monthly temperature dataset, version 4. *J. Clim.* **31**, 9835–9854 (2018).
20. Rohde, R. et al. A new estimate of the average Earth surface land temperature spanning 1753 to 2011. *Geoinform. Geostat.* **1**, 1000101 (2013).
21. Osborn, T. J. et al. Land surface air temperature variations across the globe updated to 2019: The CRUTEM5 data set. *J. Geophys. Res. Atmos.* **126**, e2019JD032352 (2021).
22. Lenssen, N. J. L. et al. Improvements in the GISTEMP uncertainty model. *J. Geophys. Res. Atmos.* **124**, 6307–6326 (2019).
23. Büntgen, U. et al. The influence of decision-making in tree ring-based climate reconstructions. *Nat. Commun.* **12**, 3411 (2021).
24. Schneider, L. et al. Revising midlatitude summer temperatures back to A.D. 600 based on a wood density network. *Geophys. Res. Lett.* **42**, 4556–4562 (2015).
25. Stoffel, M. et al. Estimates of volcanic-induced cooling in the Northern Hemisphere over the past 1,500 years. *Nat. Geosci.* **8**, 784–788 (2015).
26. Wilson, R. et al. Last millennium Northern Hemisphere summer temperatures from tree rings: Part I: the long term context. *Quat. Sci. Rev.* 1–18 (2016).
27. Guillet, S. et al. Climate response to the Samalás volcanic eruption in 1257 revealed by proxy records. *Nat. Geosci.* **10**, 123–128 (2017).
28. Büntgen, U. et al. Prominent role of volcanism in Common Era climate variability and human history. *Dendrochronologia* **64**, 125757 (2020).
29. Büntgen, U. et al. Cooling and societal change during the Late Antique Little Ice Age from 536 to around 660 AD. *Nat. Geosci.* **9**, 231–236 (2016).
30. Esper, J. et al. Large-scale, millennial-length temperature reconstructions from tree-rings. *Dendrochronologia* **50**, 81–90 (2018).

31. Esper, J. et al. European summer temperature response to annually dated volcanic eruptions over the past nine centuries. *Bull. Volcanol.* **75**, 736 (2013).
32. Esper, J., Büntgen, U., Hartl-Meier, C., Oppenheimer, C. & Schneider, L. Northern Hemisphere temperature anomalies during the 1450s period of ambiguous volcanic forcing. *Bull. Volcanol.* **79**, 41 (2017).
33. Esper, J. et al. Orbital forcing of tree-ring data. *Nat. Clim. Change* **2**, 862–866 (2012).
34. Cai, W. et al. ENSO and greenhouse warming. *Nat. Clim. Change* **5**, 849–859 (2015).
35. Huang, B. et al. Extended Reconstructed Sea Surface Temperature, version 5 (ERSSTv5): upgrades, validations, and intercomparisons. *J. Clim.* **30**, 8179–8205 (2017).
36. Columbia Climate School. ENSO forecast. *Columbia Climate School* (20 May 2024).
37. Kumar, A. & Hoerling, M. P. The nature and causes for the delayed atmospheric response to El Niño. *J. Clim.* **16**, 1391–1403 (2003).
38. Bluth, G. J., Doiron, S. D., Schnetzler, C. C., Krueger, A. J. & Walter, L. S. Global tracking of the SO₂ clouds from the June, 1991 Mount Pinatubo eruptions. *Geophys. Res. Lett.* **19**, 151–154 (1992).
39. Parker, D. E., Wilson, H., Jones, P. D., Christy, J. R. & Folland, C. K. The impact of Mount Pinatubo on world-wide temperatures. *Int. J. Climatol.* **16**, 487–497 (1996).
40. Self, S. & Rampino, M. R. The 1963–1964 eruption of Agung volcano (Bali, Indonesia). *Bull. Volcanol.* **74**, 1521–1536 (2012).
41. Francis, P. & Oppenheimer, C. *Volcanoes* 2nd edn (Oxford Univ. Press, 2004).
42. Medhaug, I., Stolpe, M. B., Fischer, E. M. & Knutti, R. Reconciling controversies about the 'global warming hiatus'. *Nature* **545**, 41–47 (2017).
43. Karl, T. R. et al. Possible artifacts of data biases in the recent global surface warming hiatus. *Science* **348**, 1469–1472 (2015).
44. Wild, M. et al. Global dimming and brightening: a review. *J. Geophys. Res. Atmos.* **114**, D00D16 (2009).
45. Stern, D. I. Reversal of the trend in global anthropogenic sulfur emissions. *Glob. Environ. Change* **16**, 207–220 (2006).
46. Allan, R. P. in *Climate Change 2021: The Physical Science Basis. Contribution of Working Group I to the Sixth Assessment Report of the Intergovernmental Panel on Climate Change* (eds Masson-Delmotte, V. et al.) (Cambridge Univ. Press, 2021).
47. Anchukaitis, K. J. & Smerdon, J. E. Progress and uncertainties in global and hemispheric temperature reconstructions of the Common Era. *Quat. Sci. Rev.* **286**, 107537 (2022).

Publisher's note Springer Nature remains neutral with regard to jurisdictional claims in published maps and institutional affiliations.

Springer Nature or its licensor (e.g. a society or other partner) holds exclusive rights to this article under a publishing agreement with the author(s) or other rightsholder(s); author self-archiving of the accepted manuscript version of this article is solely governed by the terms of such publishing agreement and applicable law.

© The Author(s), under exclusive licence to Springer Nature Limited 2024

Methods

Observed temperatures

Gridded ($1^\circ \times 1^\circ$) monthly temperatures from Berkeley Earth²⁰ were used to aggregate JJA mean temperatures over the 30–90°N land areas (<https://doi.org/10.17605/OSF.IO/MDUVK>). These data are highly similar to other products^{21,22} (Extended Data Fig. 1) and may represent the Northern Hemisphere extra-tropical land areas with reasonable instrumental station coverage back to 1850 (ref. 19). The data were expressed as residuals from the 1850–1900 mean to estimate temperature deviations from these early instrumental conditions. The variance of the 30–90° N land-only observational record is substantially larger compared with the 90° S–90° N land and sea surface temperatures⁴⁸ referred to in the 2015 Paris Agreement (Extended Data Fig. 2).

Reconstructed temperatures and adjustment

The observed temperatures were extended back over the past 2,000 years using the community ensemble reconstructions for the Northern Hemisphere extra-tropics integrating the nine longest temperature-sensitive tree-ring chronologies currently available²³ (data accessed using the KNMI Climate Explorer at <https://climexp.knmi.nl/start.cgi>). The 15 ensemble members and the mean were scaled⁴⁹ against the Berkeley Earth 30–90° N JJA observational record from 1901 to 2010 to estimate pre-instrumental temperature variability back to CE 1. The variance among the ensemble members was used to approximate 95% confidence limits, and the annually resolved temperature deviations and uncertainties from the 1850–1900 mean were considered for comparison with observational data. The 1850–1900 offset between the reconstructed and observed JJA temperatures (0.24 °C; Extended Data Fig. 3) was included in the 2023 temperature estimates to acknowledge the warm bias in early instrumental temperatures⁶ (Table 1).

El Niño Southern Oscillation and surface radiation variability

Variability of the El Niño Southern Oscillation was approximated using the central Pacific Niño3.4 sea surface temperatures³⁵ expressed as anomalies with respect to the 1891–1920 mean. This index of El Niño Southern Oscillation variability was compared over the most recent 60 years from 1964 to 2023 with the Northern Hemisphere extra-tropical JJA temperature record. In doing so, we highlighted Niño3.4 sea surface temperatures exceeding +2 °C to indicate strong El Niño conditions (except for the early 1965–1966 El Niño reaching only +1.95 °C) that probably affected global temperature deviations. The period before the mid-1980s was characterized by a reduction in surface solar radiation recorded at long-term observatory stations across the Northern Hemisphere designated^{50,51} global dimming⁴⁴.

Extended Data

We used Berkeley Earth gridded JJA land temperatures from 30° N to 90° N as these data extend back to 1850 (ref. 20) and, therefore, support assessments with respect to the 1850–1900 pre-instrumental levels referred to in the 2015 Paris Agreement. The data are compared with other gridded products (CRUTEM5 and GISTEMP)^{21,22} over their common period from 1883 to 2023 to illustrate their covariance (Extended Data Fig. 1). Berkeley 30°–90° N JJA temperatures are further compared with global annual mean land temperatures and sea surface temperatures⁵² from 1850 to 2023 to emphasize variance and trend differences (Extended Data Fig. 2). The 1850–2023 standard deviations of these timeseries differ by 0.08 °C, from 0.40 °C for the global to 0.48 °C for the sub-hemispheric temperatures.

The ensemble mean reconstruction used here to estimate the pre-Anthropocene-to-2023 range correlates at $r = 0.76$ with Berkeley Earth 30°–90° N land-only summer temperatures back to 1850 (Extended Data Fig. 3). The reconstruction is further calibrated against

high-resolution GISTEMP4 land-only and land and marine temperatures²² to show the covariance patterns across the globe (Extended Data Fig. 4). Note that the degrees of freedom of such calculations are constrained by the high autocorrelations inherent to the proxy and observational data. Detailed calibration and verification statistics of the 15 community ensemble members and the mean against various gridded temperature products are previously reported²³.

Comparison of the ensemble mean reconstruction and target of the Northern Hemisphere extra-tropical summer temperatures shows a nineteenth-century offset of 0.24 °C between early instrumental and proxy data (horizontal lines in Extended Data Fig. 3). This observation is in line with the spatial assessments of the Northern Hemisphere observational data⁶ reporting a warm bias in the sparse early instrumental network affecting the 1850–1900 baseline temperatures used in the 2015 Paris Agreement. The bias is acknowledged here by showing the proxy and observational data with respect to the 1850–1900 reconstruction mean and adding 0.24 °C to the pre-Anthropocene-to-2023 temperature estimates (Methods).

The ensemble mean reconstruction²³ fits other reconstructions of the Northern Hemisphere extra-tropical warm season temperatures^{24–28} (Extended Data Fig. 5). As the other reconstructions do not cover the entire Common Era, and thereby miss important deviations during the Late Antique Little Ice Age²⁹ and Roman Warm Period³³, we considered the community ensemble reconstruction to benchmark the 2023 summer warmth. The ensemble mean correlates at 0.60 with the five other reconstructions and the average correlation among all records is 0.59 from CE 750 to 2010. The variability of reconstructed temperatures differs among the reconstructions as is shown in the extreme years identified in the ensemble mean reconstruction labelled in Fig. 1b and listed in Table 1 (Extended Data Fig. 6).

Data availability

The observational data, reconstruction and uncertainty estimates are available at <https://doi.org/10.17605/OSF.IO/MDUVK>.

Code availability

None of the statistical tests applied were performed with environment-specific code.

48. Morice, C. P. et al. An updated assessment of near-surface temperature change from 1850: the HadCRUT5 data set. *J. Geophys. Res.* **126**, e2019JD032361 (2021).
49. Esper, J., Frank, D. C., Wilson, R. J. S. & Briffa, K. R. Effect of scaling and regression on reconstructed temperature amplitude for the past millennium. *Geophys. Res. Lett.* **32**, L07711 (2005).
50. Ohmura, A. Observed decadal variations in surface solar radiation and their causes. *J. Geophys. Res. Atmos.* **114**, D00D05 (2009).
51. Wild, M. Decadal changes in radiative fluxes at land and ocean surfaces and their relevance for global warming. *Wiley Interdiscip. Rev. Clim. Change* **7**, 91–107 (2016).
52. Rohde, R. A. & Hausfather, Z. The Berkeley Earth land/ocean temperature record. *Earth Syst. Sci. Data* **12**, 3469–3479 (2020).

Acknowledgements This study was supported by the ERC Advanced projects MONOSTAR (AdG 882727), the ERC Synergy project SYNERGY-PLAGUE (101118880), the Czech Science Foundation grant HYDRO8 (23-08049S), the co-funded EU project AdAgriF (CZ.02.01.01/00/22_008/0004635) and the Centre for Interdisciplinary Research (ZIF) in Bielefeld, Germany. We thank C. Oppenheimer, J. Quaaas and M. Wild for their discussions of volcanic and solar radiation forcings.

Author contributions J.E., M.T. and U.B. designed the study. J.E. and M.T. conducted the analyses with support from U.B. The paper was written by J.E. together with M.T. and U.B.

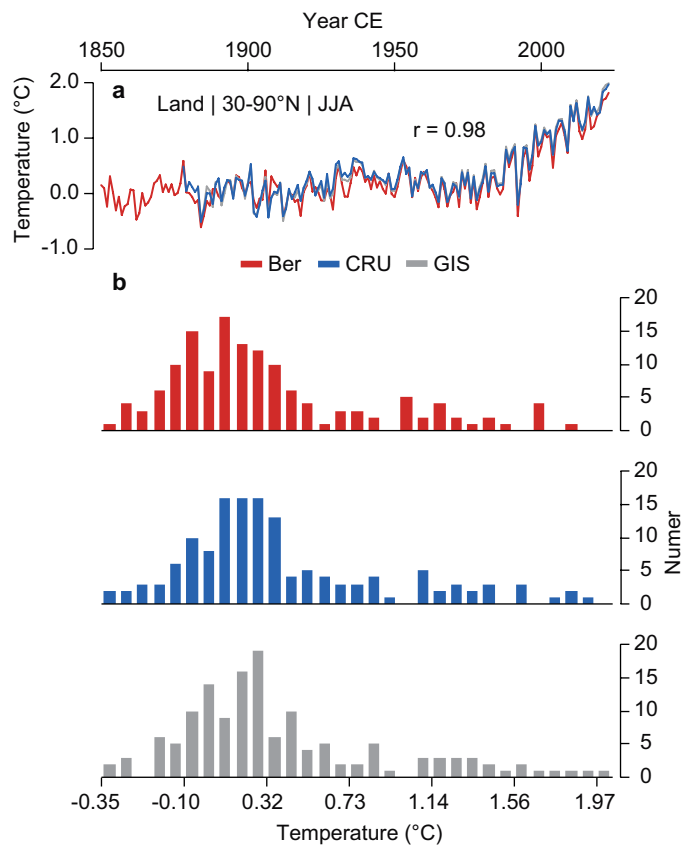
Competing interests The authors declare no competing interests.

Additional information

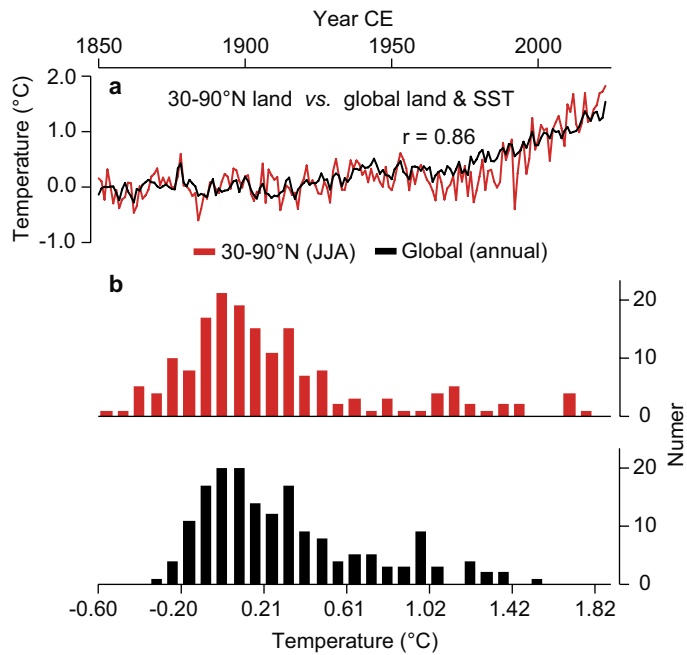
Correspondence and requests for materials should be addressed to Jan Esper.

Peer review information Nature thanks Gabriele Hegerl and the other, anonymous, reviewer(s) for their contribution to the peer review of this work.

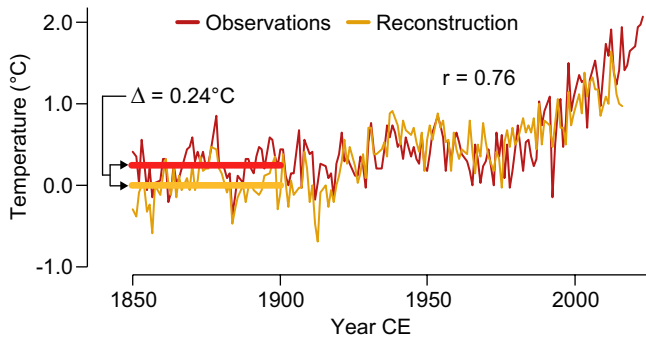
Reprints and permissions information is available at <http://www.nature.com/reprints>.



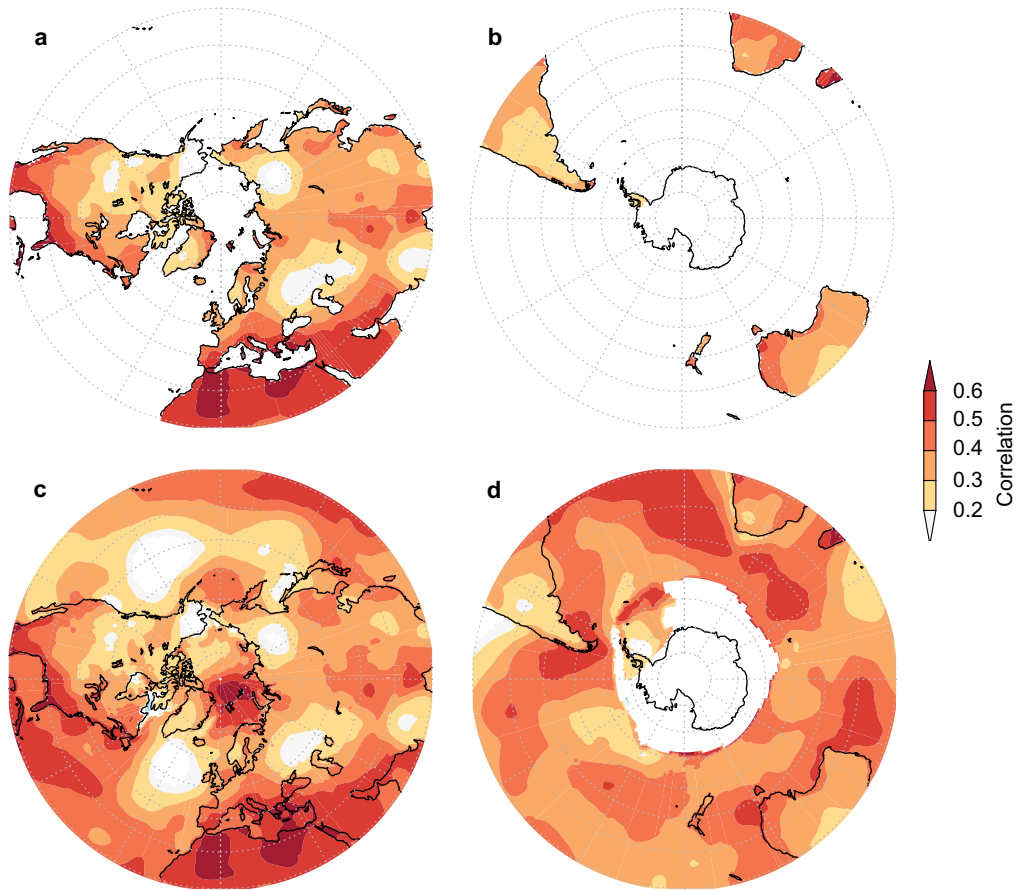
Extended Data Fig. 1 | Instrumental temperature records. a. Comparison of 30–90°N JJA land only temperatures from Berkeley Earth extending back to 1850 CE (red)²⁰, CRUTEM5 back to 1878 CE (blue)²¹ and GISTEMP4 back to 1883 CE (grey)²². **b.** Frequency distributions of the three observational records. All data shown as anomalies with respect to 1883–1912 CE means.



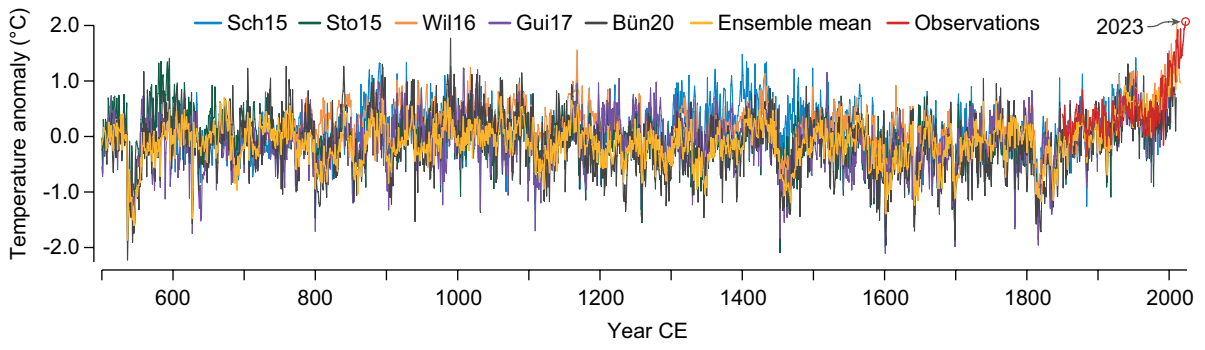
Extended Data Fig. 2 | Observational temperatures averaged over different spatiotemporal domains. **a**, Northern Hemisphere JJA land only temperatures (red) shown together with global annual land and sea surface temperatures from 1850–2023 CE (black)²⁰. The latter represents a combination of Berkeley Earth land and HadSST3 sea surface temperatures⁵². **b**, Frequency distributions. Data shown as anomalies with respect to their 1850–1900 CE means.



Extended Data Fig. 3 | Early instrumental temperature offset. Comparison of Berkeley Earth 30–90°N JJA land only observational temperatures²⁰ with ensemble mean reconstructed JJA temperatures²³ since 1850 CE. Bold horizontal lines emphasize the 1850–1900 CE offset of 0.24 °C between the two records. The reconstruction was scaled against the observations from 1901–2010 CE and both timeseries then displayed as anomalies with respect to the 1850–1900 CE reconstruction mean.

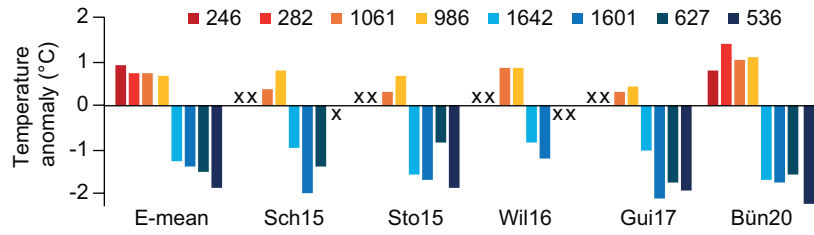


Extended Data Fig. 4 | Ensemble reconstruction climate signals. Field correlations of the ensemble mean²³ against GISTEMP4 JJA land (a, b) and land and sea surface temperatures (c, d) from 1850–2010 CE. Maps produced using the KNMI Climate Explorer at <https://climexp.knmi.nl/start.cgi>.



Extended Data Fig. 5 | Reconstruction verification. Ensemble mean shown together with other NH extra-tropical summer temperature reconstructions (ref. 24. is Sch15, ref. 25. is Sto15, ref. 26. is Wil16, ref. 27. is Gui17, ref. 28. is

Bün20) since 500 CE. All records scaled from 1901–2010 CE against 30–90°N JJA land temperatures (red) and shown as anomalies from 1850–1900 CE.



Extended Data Fig. 6 | Reconstructed temperature extremes. Comparison of temperature anomalies in the four warmest (246, 282, 1061, 986 CE) and four coldest summers (535, 627, 1601, 1642 CE) identified in ensemble mean reconstruction (see Table 1) with estimates from other NH extra-tropical reconstructions. "x" indicates if values are missing due to limited reconstruction lengths.